JOURNAL OF SPACECRAFT AND ROCKETS
Vol. 49, No. 6, November–December 2012

Tethered Coulomb Structure Applied to Close Proximity Situational Awareness

Stephen Panosian,* Carl R. Seubert,* and Hanspeter Schaub†
University of Colorado, Boulder, Colorado 80309

DOI: 10.2514/1.A32212

A unique tether application for situational awareness at geosynchronous altitudes is investigated. The relative dynamics between a small sensor platform tethered to a large host spacecraft is examined. Charging both craft to |30| kV holds the relative dynamics fixed in the presence of gravitational and solar radiation forces. Numerical simulations illustrate that the use of multiple tether connections increases the stiffness and allows 10 m separated craft to yield relative shape variations less than 50 mm in translation and 5 deg in attitude. It is also shown that in nominal plasma conditions less than 20 W of power along with only grams of propellant are required to maintain spacecraft potentials.

Nomenclature

A	=	tether cross-sectional area, m^2
$[A]$, $[B]$	=	positive definite gain matrices
A_s	=	node cross-sectional area, m^2
$[\mathcal{BI}]$	=	direction cosine matrix from inertial to body frame
C_r	=	surface reflectivity
E	=	tether Young's modulus, Pa
e_c	=	elementary charge, C
F_c	=	Coulomb force, N
F_{cc}	=	charge control force, N
$\boldsymbol{F}_g$	=	gravity force, N
$\boldsymbol{F}_{\text{SRP}}$	=	solar radiation pressure force, N
F_t	=	tether force, N
$[I]$	=	mass moment of inertia matrix, kg m^2
I_{net}	=	charge control net current, A
i, j	=	node indices
k	=	tether number indices
k_s	=	spring constant, N $\cdot$ m^{-1}
L	=	tether length, m
M	=	total number of tethers
$\dot{m}$	=	propellant mass flow rate, kg s^{-1}
m_i	=	mass of node, kg
m_{ion}, m_{electron}	=	ion and electron mass, kg
P	=	electrical power, W
P_{SRP}	=	solar radiation pressure, Pa
$\boldsymbol{p}_{ijk}$	=	tether k attachment point vector on node i, m
q	=	charge, C
$\boldsymbol{R}$	=	inertial position vector, m
r	=	distance from center, m
$\hat{S}_i$	=	unit vector from sun to node
T_e	=	electron temperature, K
$\boldsymbol{T}_{ij}$	=	total tensile force between nodes i and j, N
$\boldsymbol{u}$	=	attitude control torque, N $\cdot$ m
u_{ion}	=	charge control emission speed
V	=	potential, V
V_{SC}	=	surface potential, V
x	=	center-to-center separation, m
Γ_i	=	total body torque, N $\cdot$ m
δL	=	stretch in tether from equilibrium, m
κ	=	Boltzmann constant, J K^{-1}
λ_D	=	Debye length, m
μ	=	Earth gravitational coefficient, m^3 s^{-2}
ρ	=	sphere radius, m
$\boldsymbol{\sigma}_i$	=	modified Rodrigues parameter
$\hat{\tau}_{ijk}$	=	unit vector for tether k between nodes i and j
$\boldsymbol{\omega}_i$	=	angular velocity

Subscripts

C	=	child craft
M	=	mother craft

I. Introduction

THE time and monetary investments it takes to develop and launch a satellite to a geosynchronous orbit (GEO) prompts many precautions to be taken in satellite designs and operation. There are also risks involved with ensuring proper deployment of large structures and components on the spacecraft once at GEO. This gives rise to the need for a close proximity sensor for local situational awareness. This sensing can incorporate visual confirmation of mechanism deployment and operations as well as spacecraft and local environment information collection.

Local inspection can be an invaluable feature when diagnosing spacecraft performance or monitoring the surroundings for spacecraft and/or debris. However, actually conducting close proximity situational awareness is problematic. Japan's IKAROS (an acronym for Interplanetary Kite-Craft Accelerated by Radiation of the Sun) mission ejected a free-flying camera to obtain final images and confirmation of its solar sail deployment [1]. While providing amazing images, this ejection method allows only a single use and is not practical for GEO because it only adds to the growing space debris problem. Closed relative orbits can be used for situational awareness to keep a secondary spacecraft within a certain proximity of a primary spacecraft [2]. However, this results in the need for a complete secondary spacecraft with all major subsystems, thus increasing mission costs, mass and the risks for system failures. Additionally, this does not provide a constant relative reference point and requires significant sensing, control and propellant. These current technologies show that there is a discontinuity between what technology is available and what is needed for spacecraft close proximity operations.

Presented as Paper AAS 11-632 at the AAS/AIAA Astrodynamics Specialist Conference, Girdwood, AK, July 31–August 4, 2011; received 29 August 2011; revision received 25 January 2012; accepted for publication 25 January 2012.

*Graduate Research Assistant, Aerospace Engineering Sciences Department. Student Member AIAA.

†Associate Professor, H. Joseph Smead Fellow, Aerospace Engineering Sciences Department. Associate Fellow AIAA.

Over the past decade, several novel, essentially propellantless relative motion control concepts have been presented. These include the use of Coulomb forces [3,4], electromagnetic and flux-pinning formation flying [5–7] as well as formations maintained with Lorentz forces [8]. Of specific interest is the use of inter-spacecraft Coulomb forces to conduct close formation relative control because of its low power and propellant usage [3,4,9]. This work examines a new concept, the tethered Coulomb structure (TCS), and its use for close proximity sensing at GEO.

The TCS concept provides a means of creating semirigid structures in space using Coulomb forces and spacecraft interconnected with fine, low mass tethers [10,11]. Using continuous charge emission the spacecraft nodes are charged to kilovolt potentials and repelled, holding the tethers in tension. A benefit of the TCS system is that the interconnecting tethers restrict relative translational and rotational motions, providing a continuous close proximity platform that can be used for situational awareness. A key advantage of a TCS is that it would have long-term mission capability because, it only requires watt levels of power and low propellant mass [10]. A benefit of a TCS system over free-flying Coulomb formations is that a TCS does not require precise charge levels to maintain relative positions due to its shape being constrained by the tethers. Spacecraft charge levels must only be maintained above a certain threshold for which the TCS system would be robust to orbital perturbations such as differential gravity and solar radiation pressure (SRP). Additionally, relative attitude control between spacecraft nodes is negligible when the Coulomb and tensile forces are in equilibrium.

Using a TCS system does however have its limitations. Space plasma reduces the Coulomb force between spacecraft nodes making it challenging to implement in low Earth orbit. The plasma is characterized by the Debye length (λ_D) which at GEO is large providing minimal force shielding. Three representative, single Maxwellian, GEO plasma conditions (quiet, nominal, and disturbed) are used to define the extreme bounds and nominal operating regimes a TCS spacecraft will encounter on orbit. The properties of these plasmas are defined in a previous publication by the authors [12]. Of importance here is the corresponding Debye lengths which are directly used in the force modeling equations. The three representative GEO plasma Debye lengths are the following: quiet, $\lambda_D = 4$ m; nominal, $\lambda_D = 200$ m; and disturbed, $\lambda_D = 743$ m. The quiet plasma ($\lambda_D =$ 4 m) bounds the "worst-case" conditions at GEO and are only characteristic of extreme times. Nominal plasma conditions are a closer representation of the typical operating conditions at GEO, while a disturbed environment is the lower limit of power requirements and force shielding.

While a TCS has many mission potentials the one application analyzed here is the ability to provide a local and small sensor platform to a geosynchronous satellite. Here one large spacecraft (the mother) has a smaller spacecraft (the child) tethered to it as illustrated in Fig. 1. Both craft are spherical and feature an outer conducting surface for charge distribution. This mother–child (MC) application of a TCS can provide a unique vantage point for on-orbit inspection of the mother craft, rendezvous, docking and refueling operations and space environment measurements. The key advantage that a TCS can provide for situational awareness at GEO is that it can hold a child spacecraft at a relatively fixed position and attitude with respect to the mother craft with minimal sensing, control and propulsion needs. It is expected that the child craft is a small, low mass craft with only minimal or essential hardware.

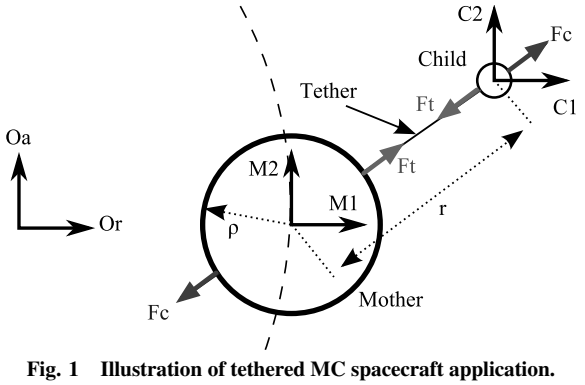

Fig. 1 Illustration of tethered MC spacecraft application.

The intent of this paper is to explore this specific application of the TCS concept. This involves quantifying the plausible MC operating configurations and the resulting dynamics and power requirements to maintain potential. Previous research on the TCS concept investigates relative motion without nodal rotation [10] as well as simplified two-dimensional translational and rotational motion about one axis [11]. A full three-dimensional study is conducted for two identical TCS nodes [12], but does not simulate naturally unstable on-orbit configurations or large mass ratios. This study expands upon these previous research endeavors by simulating two nonidentical (size or mass) TCS nodes (mother and child) in naturally unstable orbit configurations.

This paper features spacecraft that are modeled as spherical conductive shells. Using conductive spheres results in an even charge distribution and produces line of sight Coulomb force between sphere centers to isolate dynamic responses. There are challenges to be investigated and overcome to use charged craft and achieve the concept of Coulomb formation flight. These challenges include differential charging of insulator materials and discharging, the associated electromagnetic interferences and possible issues with communications, and maintaining an unbiased sensing platform in the presence of a charged spacecraft. One method of achieving an outer conductive surface, on nonmetallic objects, and prevent differential charging is being investigated with transparent coatings such as indium tin oxide [13]. The concerns associated with the full technical implementation are beyond the scope of study of this paper.

The objectives of this work and an outline of this paper is as follows. Of interest is the extent of relative rotation and translation between the mother and child craft. The influential forces and equations of motion for a TCS are presented along with the parameters of the MC baseline application. Numerical simulation results are presented to show plausible MC operating regimes and resulting dynamics. The effects of spacecraft potential on required power and dynamics is studied. An overview of current technological means of charging spacecraft is given along with estimates on the propellant mass needed to maintain MC operational potentials in a plasma. Lastly, the mass of the child craft is investigated to quantify its effects on the MC relative dynamics.

II. Equations of Motion

This section develops the Coulomb force between the charged mother and child craft in a plasma and presents the resulting translational and rotational equations of motion for this TCS application.

A. Electrostatic Force Modeling

A Coulomb force is generated from the electrostatic interaction of two charged bodies. Consider the isolated mother that is a finite sphere of radius ρ_M. It is in a plasma and holding a surface potential V_M so the surrounding potential field can be represented by the Debye–Hückel equation [14,15]:

$$V(x) = \frac{V_M \rho_M}{x} e^{-(x-\rho_M)/\lambda_D} \tag{1}$$

Here x is the separation distance to the center of the sphere. This equation is only valid if a small spacecraft potential compared to the local plasma thermal energy is assumed ($e_c V \ll \kappa T_e$), where $e_c = 1.602176 \times 10^{-19}$ C is the elementary charge, $\kappa = 1.38065 \times 10^{-23}$ J · K^{-1} is the Boltzmann constant and T_e is the plasma electron temperature in Kelvin. In a nominal GEO plasma the ($e_c V \ll \kappa T_e$) condition is no longer true if the spacecraft charges to >1–10 kV potentials. The Debye–Hückel equation is derived from neglecting the higher order terms of Poisson's partial differential equation which

results in less plasma shielding of the electrostatic fields, and represents a conservative estimate [16]. The benefit of using Eq. (1) is that it allows for simplified analysis, and faster numerical simulations because the full Poisson–Vlasov equations do not need to be solved. Solving the full Poisson–Vlasov equations requires solving complex partial differential field equations and is not used here over the conservative analytic approximation. For the nominal 200 m Debye length plasma the accuracy of the Debye–Hückel approximation is within 5% of a numerically computed value.

Equation (1) is differentiated to obtain the electric field (E field) of the isolated sphere and rearranged to obtain the relationship between charge and potential in a plasma:

$$V_M = \frac{q_M k_c}{\rho_M}\left(\frac{\lambda_D}{\rho_M + \lambda_D}\right) \tag{2}$$

If this plasma has minimal interaction ($\rho_M \ll \lambda_D$) this charge on the isolated sphere reduces to the classical vacuum formulation ($V = qk_c/\rho$) as required. If a second charge q_C (child) is placed at a distance r in the E field of the mother the resulting Coulomb force, which is also a conservative estimate [16] is computed using [12]

$$|\boldsymbol{F}_c| = k_c \frac{q_M q_C}{r^2} e^{(-(r-\rho_M))/\lambda_D}\left(1 + \frac{r}{\lambda_D}\right) \tag{3}$$

where $k_c = 8.99 \times 10^9\ \mathrm{N \cdot m^2 \cdot C^{-2}}$ is the vacuum Coulomb constant. To account for the influence of charged finite spheres in close proximity in this Coulomb force equation it is necessary to compute the combined capacitance of the system. This is achieved by using the potential of the mother [Eq. (2)] and including the potential of the child craft [17,18], at a distance r, using the child equivalents of Eqs. (1) and (2) giving the relationship of the MC system:

$$V_M = \frac{q_M k_c}{\rho_M}\left(\frac{\lambda_D}{\rho_M + \lambda_D}\right) + \frac{k_c q_C}{r}\left(\frac{\lambda_D}{\rho_C + \lambda_D}\right) e^{-(r-\rho_C)/\lambda_D} \tag{4}$$

where ρ_C is the radius of the child. Similarly, there is an equivalent potential equation for the child and combined we obtain a system of linear equations:

$$\begin{bmatrix} V_M \\ V_C \end{bmatrix} = k_c \begin{bmatrix} \frac{1}{\rho_M}\left(\frac{\lambda_D}{\rho_M+\lambda_d}\right) & \frac{1}{r} e^{\frac{-(r-\rho_C)}{\lambda_D}}\left(\frac{\lambda_D}{\rho_C+\lambda_D}\right) \\ \frac{1}{r} e^{\frac{-(r-\rho_M)}{\lambda_D}}\left(\frac{\lambda_D}{\rho_M+\lambda_D}\right) & \frac{1}{\rho_C}\left(\frac{\lambda_D}{\rho_C+\lambda_D}\right) \end{bmatrix} \begin{bmatrix} q_M \\ q_C \end{bmatrix} \tag{5}$$

The simulations for this study specify a constant and equivalent potential $V_M = V_C$ for the spacecraft, which is a nominal TCS application characteristic. Using this desired potential, Eq. (5) is inverted to solve for the resulting charges which are used to compute the repulsive Coulomb force using Eq. (3). With fixed surface potentials, this combined capacitance has a significant influence on the effective charge of each sphere, when the center-to-center separation is low relative to the sphere radii (separations less than approximately 10 sphere radii, ($r < 10\rho$). Uneven charge distribution on the conducting spacecraft surfaces is not considered in this analysis as it is only significant for very close separations ($r < 3\rho$). The interaction of a charged craft with the geomagnetic field, and the resulting Lorentz force, is not included in this analysis as the craft are in GEO with zero relative velocity to the field.

B. TCS Forces

The numerical simulation of this study computes the translational and rotational motion of TCS nodes. The only forces assumed to be acting on a TCS at GEO are Coulomb, tensile, gravity, and SRP.

The tethers are modeled as a proportional spring with nonlinear end displacements. This allows for general tether stretching due to arbitrary node translation and/or rotation. The magnitude of the tensile force from a single tether is given by

$$|\boldsymbol{F}_s| = \begin{cases} k_s \delta L & \delta L > 0, \\ 0 & \delta L \le 0 \end{cases} \tag{6}$$

where k_s is the proportional spring constant and δL is the stretch in the tether. The spring constant is computed from the tether properties using the relationship ($k_s = EA/L$) where E, A and L are Young's modulus, tether cross-sectional area and the nominal tether length, respectively. For this work E and A are assumed to be 271×10^9 Pa and 5.29×10^{-10} m^2, respectively. These parameters are representative of the fine, low mass tether materials currently being considered for a TCS.

If the MC system features only a single connecting tether, Eq. (6) gives the total tether force on each node. However, the algorithm is capable of simulating multiple tethers between each node. The tether length increase of tether k between nodes i and j is defined by δL_{ijk}. Therefore, the resulting tensile force acting on node i from the tether (s) connected to node j is

$$\boldsymbol{T}_{ij} = k_s \sum_{k=1}^{M} \delta L_{ijk} \hat{\tau}_{ijk} \tag{7}$$

where M is the number of tethers between nodes i and j and $\boldsymbol{\tau}_{ij}$ is the vector defining the kth tether's connection between node i to j.

A two-body gravity model is simulated for the TCS operating at GEO with a force:

$$|\boldsymbol{F}_g| = \frac{\mu m_i}{|\boldsymbol{R}_i|^2}\hat{R}_i \tag{8}$$

where $\mu = 3.986 \times 10^{14}\ \mathrm{m^3 \cdot s^{-2}}$ is the gravitational coefficient for Earth, m_i is the spacecraft node mass and $\boldsymbol{R}_i$ is the inertial position of node i.

The SRP force at 1 AU is simulated using

$$\boldsymbol{F}_{\mathrm{SRP}i} = P_{\mathrm{SRP}} C_r A_s \hat{S}_i \tag{9}$$

where P_{SRP}, C_r, and A_s are the SRP, surface reflectivity and the cross-sectional area of the spacecraft, respectively and $\hat{S}_i$ is the unit vector from the sun to node i.

C. Translational Equations of Motion

All four forces simulated at GEO (Coulomb, tensile, gravity and SRP) are included in the translational equations of motion of a TCS node:

$$\ddot{\boldsymbol{R}}_i = -\frac{\mu}{|\boldsymbol{R}_i|^2}\hat{R}_i + P_{\mathrm{SRP}} C_r A_s \hat{S}_i + \frac{\boldsymbol{T}_{ij}}{m_i} + \frac{k_c q_i q_j (-\hat{r}_{ij})}{m_i r_{ij}^2} e^{(-(r_{12}-\rho))/\lambda_D}\left(1 + \frac{r_{ij}}{\lambda_D}\right), \qquad i \neq j \tag{10}$$

D. Rotational Equations of Motion

It is assumed that the only torque driving the rotational motion of a TCS node is from the tether forces. Differential gravity and SRP induced torques can be ignored because the spacecraft are spherical and have symmetric mass moments of inertia. With even charge distribution on the conducting spheres the Coulomb forces act on the center of each node producing no torque. Previous studies looked at varying the symmetric mass moment of inertia on nodal dynamics [12]. A mass moment of inertia of a solid sphere is used in this study to isolate the dynamics of the coupled system without further complication. The attitude of each spacecraft node is dependent on the torque from each tether:

$${}^{B}\Gamma_i = \sum_{k=1}^{M} ({}^{B}\boldsymbol{p}_{ijk} \times [\mathcal{BI}]_i^I \boldsymbol{T}_{ijk}), \qquad i \neq j \tag{11}$$

where $\boldsymbol{p}_{ijk}$ is the body fixed vector that defines the location of the kth tether attachment point on node i that connects to node j and $[\mathcal{BI}]_i$ is the direction cosine matrix of the attitude of node i relative to the inertial frame. The angular acceleration of each node is defined in the body frame with Euler's rotational equations of motion [2]:

$$[I]_i\dot{\boldsymbol{\omega}}_i = -\boldsymbol{\omega}_i \times ([I]_i\boldsymbol{\omega}_i) + \Gamma_i \tag{12}$$

The attitude of each node is represented with the modified Rodrigues parameters (MRP) which are integrated using the differential kinematic equation:

$$\dot{\boldsymbol{\sigma}}_i = \frac{1}{4}[(1-\sigma_i^2)[I_{3\times3}]_i + 2[\tilde{\boldsymbol{\sigma}}]_i + 2\boldsymbol{\sigma}_i\boldsymbol{\sigma}_i^T]\boldsymbol{\omega}_i \tag{13}$$

The MRP set will go singular with a rotation of $\pm$360 deg. To ensure a nonsingular description, the MRP description is switched to the shadow set whenever $|\boldsymbol{\sigma}| > 1$ [2].

III. Mother–Child Configuration

This section outlines the parameters of a baseline two node, MC configuration used for simulations and presents both natural and controlled dynamics of this TCS application. The trivial set up for this MC configuration is to have the two craft in a orbit radial alignment. Under differential gravity, this set up would maintain a taut tether and constant shape without charge, but would be less robust to perturbations. Charging the spacecraft allows for additional orbit configurations and reduces relative translation and rotation motions. This section uses numerical simulations to examine the requirements of a TCS to hold a child craft fixed relative to the mother in an arbitrary orbit configuration. Unless otherwise stated, the mother and child are modeled as spheres with masses and radii of 2000 kg, 2 m, 50 kg, and 0.5 m, respectively. All other baseline simulation parameters are listed in Table 1. Additionally, the spacecraft system begins each simulation with an inertial rotation rate equal to that of the orbit frame (360 deg per day).

A. Tethered Structure vs TCS

A configuration of more interest than an orbit radial alignment, is when the child is placed at an arbitrary position relative to the mother craft. One such example would be placing the child craft where it would have positive radial and along track components relative to the mother craft. Figure 2 graphically shows time elapsed snapshots of a tethered structure (TS) and TCS for this baseline two node system with system parameters given in Table 1. From Fig. 2 it can be seen that for a TS (left) the relative position and attitude of the two craft varies over an orbit from an initial stationary relative separation and attitude. The tether is mostly slack and after only 5 hs there is a significant relative rotation between the child and mother. The TCS (right) however, maintains a reasonably fixed relative position and rotation between the two craft. Figure 3 shows numerically the small relative position and rotation difference between the mother and child craft in this simulation. The relative attitude here and in all subsequent simulations is calculated as the Euler principal rotation about the principal axis. The reason for the small relative motion deviations is that the tether between the two craft remains almost always in tension throughout the orbit. The constant tension restricts the variations in relative distance and rotation to less than 4 mm and 1 deg, respectively. Thus, this shows a single-tether TCS can be used to hold a child craft relatively fixed in relation to a mother spacecraft. These results are also typical if the child craft has an out of plane position, relative to the mother craft.

Table 1 MC baseline simulation parameters

Parameter	Value
Nodal surface potential	30 (kV)
Center-to-center separation	7 (m)
Mass moment of inertia	Solid sphere
Tether spring constant	35.8398 (N · m^{-1})
Debye length λ_d	200 (m)
SRP at 1 AU P_{srp}	4.56×10^{-6} (N · m^{-2})
Surface reflectivity C_r	1
Simulation duration	24 h

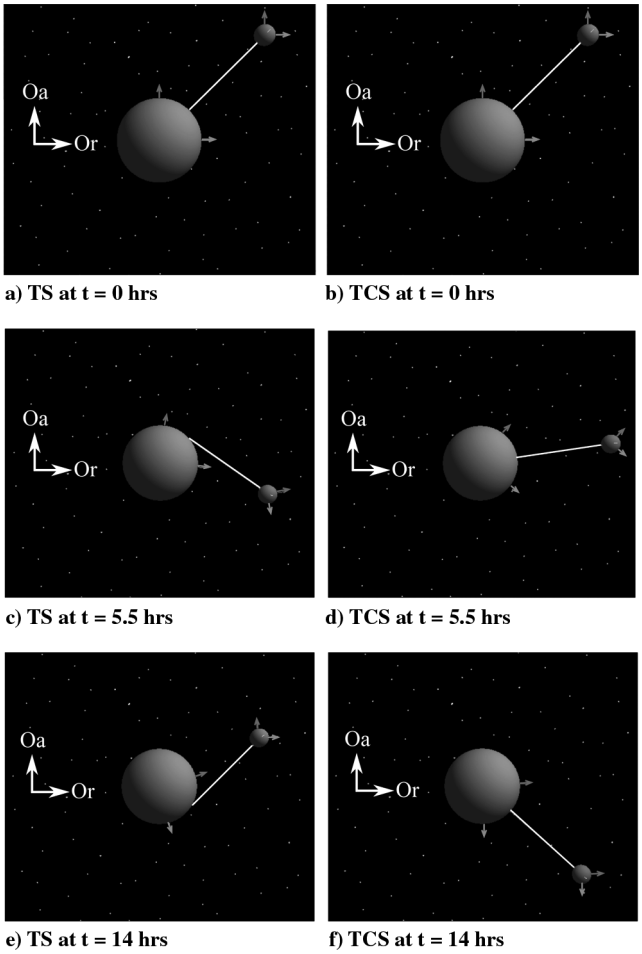

Fig. 2 Comparison of MC relative motions with and without Coulomb repulsion.

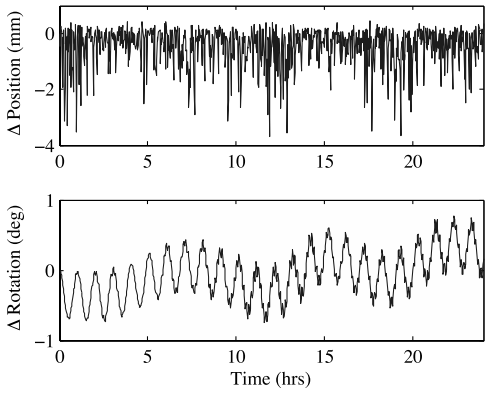

Fig. 3 TCS MC relative position and rotation from orbital perturbation.

B. Fixed Mother Craft

Figure 3 shows that the relative positions and rotations between a mother and child TCS can be kept nearly constant for arbitrary initial orbit alignment. However, the system as a whole does undergo rotation relative to the orbit frame. This contradicts a common GEO attitude requirement to remain fixed relative to the orbit frame. This can be addressed by implementing a simple and stable attitude control solution to fix the mothers pointing in the orbit frame using

$$\boldsymbol{u} = -[A]\boldsymbol{\sigma} - [B]\boldsymbol{\omega} \tag{14}$$

where $[A]$ and $[B]$ are positive definite gain matrices [2]. Including this control in the mother's rotational equations of motion of Eq. (12) gives

$$[I]_M\dot{\boldsymbol{\omega}}_M = -\boldsymbol{\omega}_M \times ([I]_M\boldsymbol{\omega}_M) + \Gamma_M + \boldsymbol{u} \tag{15}$$

This control torque, $\boldsymbol{u}$, is assumed to be applied by an internal momentum wheel system on the mother craft. Figure 4 shows the relative numerical results for a MC configuration implementing the control of Eq. (14). In this scenario the mother craft orientation is held fixed, while the tethered child spacecraft is free to translate and rotate due to the differential gravity, SRP, Coulomb and tether forces. Of interest is the magnitude of the relative child motions in this scenario. The parameters for this simulation are given in Table 1 and the control is implemented at 1 Hz with gains of 100. These gains are chosen based on predicted performance to hold the mother craft fixed in the orbit frame. This control torque is implemented in all future simulations.

From Fig. 4a it can be seen that the child craft relative position initially moves in the positive radial and negative along track directions, which is expected for a craft with an initially larger orbit. However, this motion is restricted by the tether and causes oscillations less than 80 mm in each direction. The top plot in Fig. 4b shows the relative rotation between the child and mother craft, while the bottom plot illustrates the rotation of the mother craft relative to the orbit frame. From the figure it can be seen that this simple control holds the mother aligned with the orbit frame and subsequently the child orientation is held within 1 deg of the mother. As expected, with the controlled mother attitude case the relative translational motion is larger magnitude than with the uncontrolled mother attitude scenario. However this relative motion is still small at less than 80 mm at these charge levels. These results define the baseline constrained relative motions for the MC TCS setup. It is now beneficial to examine the effect of deviations in separation distances from this baseline MC configuration on the relative motion.

C. Relative Dynamics due to Separation Distance Variations

The distance between the mother and child craft determines what operations the child can perform, as well as what field of view the child has of the mother. The larger the separation distance between the two, the greater field of view the child has of the mother and surroundings for inspections and situational awareness. Of interest in this study is the effect of varying separation distance on the relative motions of the MC nodes. To obtain the most complex relative dynamics the child craft is initially positioned with equal proportions in the mother's local radial, along and cross track directions.

In addition to varying the separation distances, additional tethers between the spacecraft nodes are implemented to examine enhanced relative motion constraints. An investigation into enhancing rotational stiffness with additional tethers in shown in [12]. It is demonstrated that a tether connection angle of 45 deg (angle at sphere center between tether connection point and vector to second sphere) is a suitable compromise between increased stiffness and rotational margin from wrap-up. A tether connection angle of 45 deg is therefore used in this analysis.

Figure 5 shows the maximum relative rotation between the mother and child, maximum variation in separation distance and required control torques for various MC separation distances. These results serve as a measure of the stiffness of a MC TCS. All three plots in Fig. 5 show that increasing separation distance increases the maximum relative rotation, the maximum separation from equilibrium and the required torque. The required torque is the total net sum for an entire 24 h orbit and Fig. 5c shows that the amount required is well within what is feasible with current momentum wheel systems on a GEO spacecraft.

Figures 5a and 5b show that increasing the tether number reduces rotations and variations in separation distance of the MC TCS. Using a triple tether configuration can reduce the maximum relative rotation by up to 60% (at a 15 m separation). Figure 5a demonstrates that separation distances upwards of 10 m can still provide reasonable relative rotations of about five degrees for this scenario with the child in the radial, along and cross track directions. Additionally, the results of Fig. 5b show that there will only be centimeter level variations in separation distance between the two craft.

IV. MC Power Requirements and Potential Considerations

The previous section shows that constrained relative motion between a mother and child can be achieved for an arbitrary orbit orientation. However, in addition to the implemented control torque, it is also required that the spacecraft maintain elevated potentials for all time. While there are technological challenges to overcome to maintain long-term kilovolt potentials, this fundamental study gives a measure of the plasma and spacecraft interaction. It estimates the resulting power needs to maintain a TCS at desired potentials in GEO space plasma conditions. Additionally, the effects of the spacecraft polarity on the required power is examined for various potentials. Lastly, the net result of varying the spacecraft potential on the relative dynamics of the MC TCS is investigated.

A. Coulomb Power Requirements

The net power required for a charged spacecraft to maintain a fixed potential in a plasma is directly proportional to the spacecraft potential and the net current from the plasma. This is represented with $P = V_{sc}I_{net}$, where V_{sc} is the spacecraft potential relative to the plasma and I_{net} is the net plasma current. It is assumed in this analysis that the charge emission current has sufficient energy to escape the charge of the craft. Additionally, for the purposes of this calculation local plasma alterations and sheath effects, such as seen on the high intentional charging of Space Power Experiment Aboard Rockets (SPEAR 1) [19,20], are omitted.

The plasma is modeled as two populations (electrons and protons) with single-Maxwellian distributions. A spacecraft at GEO is stationary relative to the plasma (no ram currents) and the two primary current contributions are from electron and ion bombard-

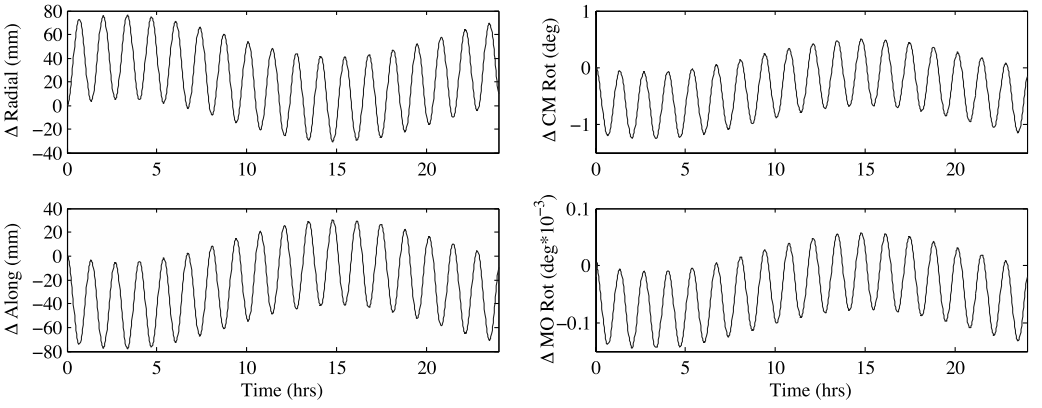

a) Relative change in position b) Child/Mother & Mother/orbit relative attitudes

Fig. 4 TCS MC relative position and rotation with mother attitude control.

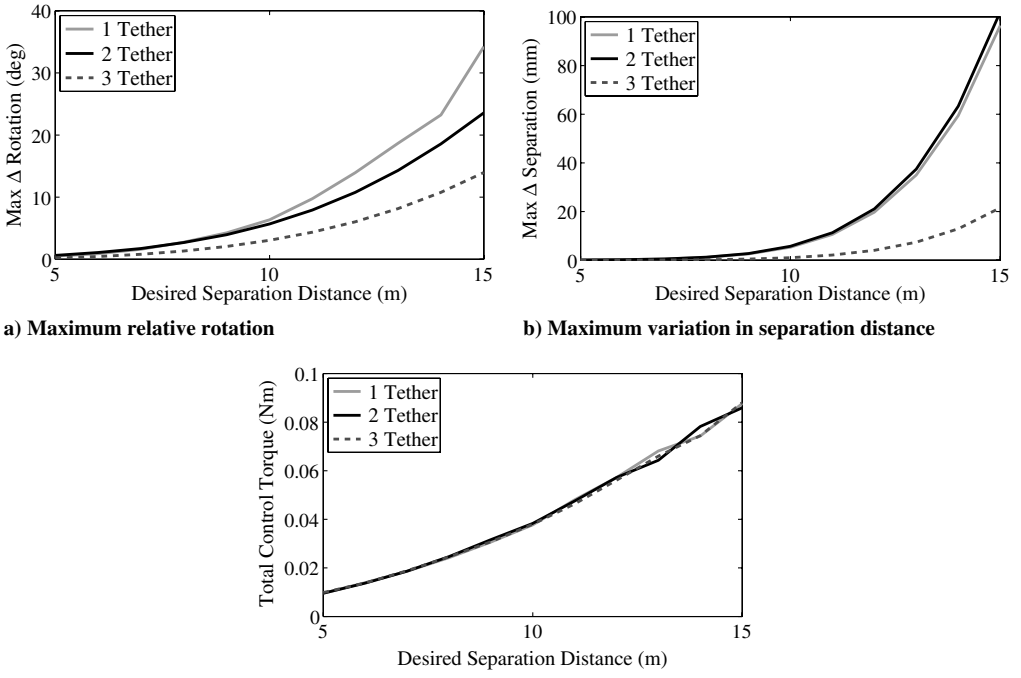

a) Maximum relative rotation

b) Maximum variation in separation distance

c) Total required attitude control torque

Fig. 5 MC relative dynamics as a function of separation distance and number of connecting tethers.

ment. The net plasma current is developed for both positive and negatively charged spacecraft in [12] using the Boltzmann factor representation and exponential repulsion and Mott–Smith and Langmuir attraction [21,22]. The net plasma current also includes a third contribution, the photoelectron current on sun-lit surfaces. For this particular study only sun-lit conditions are analyzed for power requirements as a spacecraft at GEO may be in eclipse for only minutes at a time in a 24 h orbit. However, during these minimal eclipse periods is when the spacecraft can naturally and safely charge to kilovolt potentials. A charge feature that can be used by the TCS concept.

The combined power required to equally charge both the 2 m radius mother and 0.5 m radius child for each of the plasma conditions is shown in Fig. 6. The range of spacecraft potentials used in this analysis is −30 to 30 kV, a reasonable range that is anticipated for TCS operations. The total power required of the MC system in a nominal plasma ($\lambda_d = 200$ m) is 8.2 W for −30 kV and 17.2 W for 30 kV. This is a realistic power consumption for a large GEO spacecraft. In the worst-case and rarely experienced quiet plasma ($\lambda_d = 4$ m) the power required by the system to maintain −30 kV is 181 W, and to achieve 30 kV requires 7439 W.

These power estimates are independent of the separation distances of the spacecraft. A consideration for the system is whether the mother features a single charge control device that charges both itself as well as the child through a conductive tether. An alternative is to have a charge control device on each craft that operates independently. Considering the eclipse operating environment, the craft have an equivalent power requirement during positive charging as this is independent of the photoelectron current. During negative charging, the net plasma current is lower and hence the power requirements are lower than this sun-lit case.

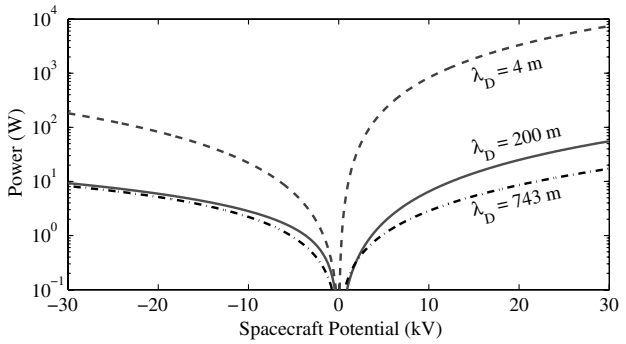

Fig. 6 Power required in sun light to maintain spacecraft potential for each plasma.

B. Potential Effects on Dynamics

In addition to its effects on power consumption, potential of the spacecraft also affects the dynamics of the MC configuration. The results of the previous section shows that lower potentials require less power, however a compromise is sought that also provides suitable constraints on the MC relative dynamics. Simulations are run to show the effects that various spacecraft potentials have on the MC dynamics. However, unlike the previous power consumption analysis, the polarity of the spacecraft does not alter the repulsion force between the two spacecraft so only positive potentials are considered. For these simulations there is an identical potential on each craft, but in practice different potentials on each craft could be used to simplify the design of either craft. Again, a worst-case orbit configuration with the child in all three orbit directions is used. All other parameters are listed in Table 1.

Figure 7 shows the maximum relative rotations and maximum variation in separation distance as a function of MC potential. Similar to the distance variation, Figs. 7a and 7b show that additional tethers decreases the maximum relative rotations and separation variations. Additionally, these figures show that increasing potentials also decreases these relative quantities. However, increasing the potential beyond 30 kV provides little improved performance, thus 30 kV can be considered a nominal maximum potential for this baseline TCS application. This magnitude of potential is also technically achievable. Potentials lower than 30 kV could be used to decrease power consumption but system stiffness decreases nonlinearly with potential. Lastly, simulation results indicate that spacecraft potential has negligible effect on the required attitude control torque and is consequently not shown. This is anticipated as the Coulomb inflation force is line of sight with no moment arm and therefore minimal variation on the required mother control torque.

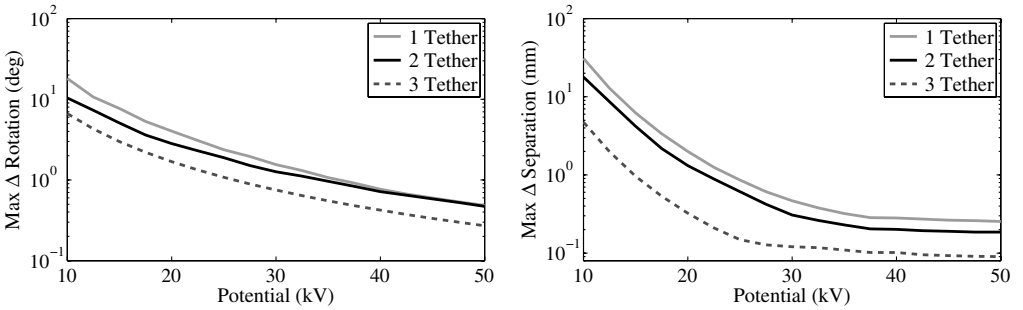

a) Maximum relative rotation **b) Maximum variation in separation distance**

Fig. 7 MC relative dynamics as a function of craft potential and number of connecting tethers.

C. Positive and Negative Charging Considerations

The previous sections show that increasing charge (Coulomb force) reduces TCS relative motions and that the power requirements are dependent on the polarity and magnitude of the craft potential. An additional consideration for both power consumption and Coulomb force is the size of the spacecraft nodes. Larger nodes generate a greater Coulomb repulsive force (for a given potential level) while also requiring a larger power requirement due to a larger surface area being bombarded by the plasma. Analyzed here is the force generation and power requirements of the baseline MC system in comparison to a equal radii, two sphere system.

The Coulomb force generated between the two spherical TCS nodes of potential V_{sc} is computed using the force of Eq. (3) with shielding from the nominal plasma ($\lambda_d = 200$ m). The total power required is also computed in this nominal plasma in sunlight (photoelectrons included). Both the force and power is shown on a common axis as a function of spacecraft potential in Fig. 8. The MC power and force is directly compared to a two node system of equal radii of three different values. In this figure the solid lines represent the required power, the dashed lines are the Coulomb force generated. This is computed in a nominal plasma ($\lambda_D = 200$ m) with a center-to-center separation of 7 m.

Both the force and power are a function of $f(r^2)$, hence at a given potential the proportional increase between each radial line is equivalent. Ultimately, there is no optimal radii, TCS nodal size should be selected based on total power limitations, mass and size constraints or minimum force required for a given potential.

The Coulomb force is a function $F_c = f(V_{sc}^2)$ which dictates the shape of the curves, and is equivalent magnitude for both positive and negative potentials. The power required during positive charging is also a function $P(V_{sc} > 0) \approx f(V_{sc}^2)$ and hence has a similar profile to the force. However during negative charging in this nominal plasma, the dominant current is the constant photoelectrons and the resulting power is a function $P(V_{sc} < 0) \approx f(V_{sc})$. The result is that for negative charging lower power is required to achieve the equivalent force at a given potential.

To demonstrate the relationship between force and power, Fig. 9 shows the ratio F_c/P for the MC baseline setup. A large ratio value indicates more force is obtained per power required. This figure shows that for positive charging the ratio is constant. Figure 9 also shows that it is more advantageous to use negative charge, as an equivalent force can be generated for less power than the same positive charge.

V. MC Propellant Mass Estimates

Another consideration for implementing a Coulomb repelled tethered child on a GEO spacecraft is the amount of additional mass. Analyzed here is the mass of charge control devices currently available and an estimate of the propellant mass required to maintain the desired surface potentials in the three representative plasma conditions (quiet, nominal, disturbed). Similar to the power analysis, the polarity of the spacecraft potentials is a factor in the propellant mass required and is investigated here. Propellant mass is calculated for the baseline MC system with 2 and 0.5 m radius spheres, respectively, operating in sunlit conditions.

A. Charging Hardware

Charging of spacecraft in a space plasma is a natural process that can be regulated or enhanced for TCS purposes using a charge emission device. Previously, Figs. 6 and 8 demonstrated that from a power perspective it is more advantageous to charge to negative potentials. Another consideration is the technology required for charge control. The technology for electron emission (positive charging) is less complex and electrons are freely available from solar energy. Alternatively, for negative charging, two primary charge control techniques that are space proven are the hollow cathodes that emit noble gas ions and field emission using metal ions. A brief overview of these charge emission devices currently used or available for space missions is given. It is envisioned that Coulomb formations and TSs will implement technology based on this space heritage hardware. Charging to kilovolt level potentials intentionally is a challenging task and while there is technology available, further advancements are necessary for the TCS concept to be fully realized.

Hollow cathode emission accelerates gaseous ions typically of argon, krypton, or xenon that are stored in tanks up to 1000 psi [23]. SCATHA is a spacecraft that used both an electron gun and a xenon ion beam for charging [24]. ProSEDS was intended for launch in

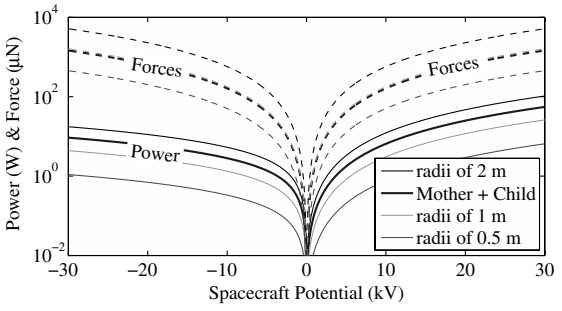

Fig. 8 Force generated and total power required in sunlight as a function of sphere potential and craft radius.

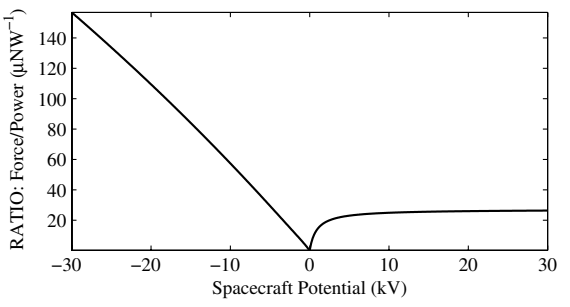

Fig. 9 Ratio between force generated and power required in sunlight and a nominal plasma.

Table 2 Combined maximum mass flow rate ($\mu g \cdot s^{-1}$) for each plasma at a given spacecraft potential

Spacecraft potential	Quiet ($\lambda_D = 4$ m)	Nominal ($\lambda_D = 200$ m)	Disturbed ($\lambda_D = 743$ m)
−30 kV	8.24	0.42	0.37
+30 kV	0.0014	1.0×10^{-5}	3.3×10^{-6}

2003 with 245 g of xenon for charge control. With a maximum emission current of 10 A at 200 μg/s, the system used 30 W, had a mass of 6 kg and dimensions of $20 \times 30 \times 13$ cm [25].

The alternate charge control device used in space is field evaporation with metal ions. The cluster spacecraft emit Indium ions from a liquid source to maintain zero potential relative to the plasma. The emission current is 10–15 μA from an instrument that consumes less than 2.7 W and has a mass of 1.85 kg [22,26]. Similarly, the Geotail spacecraft uses two Indium ion emission devices of 1.8 kg, measuring $19 \times 16 \times 17$ cm, with a current of 15 μA.

This gives an indication of the use of charge control devices in space but of importance here is the quantification of the mass, volume and power requirements of devices that could similarly be implemented on the MC TCS system.

B. Propellant Mass Flow Rates

For a TCS to maintain a fixed potential in a plasma, a charge control current is required to offset the net plasma current. The propellant mass flow rate of this charge control current is determined. As the mass flow requirements are based on charge emission current calculations shown previously, the same assumptions are used with regard to sufficient current energy and ignoring locally generated plasma plumes. To charge to negative potentials positive ions from an on board propellant source are emitted. For this study the mass flow rate, during negative charging, is computed using xenon gas ions (Xe^+). For charge control emission it is most advantageous to use the lowest mass particles (ideally H^+ ions), however xenon is used as it is a common hollow cathode propellant and it results in the largest (worst-case) mass flow rate, with a higher ion mass than Indium (a common field emission propellant) [22,27]. The mass flow rate, during negative charging, is computed using [3]

$$\dot{m} = \frac{|I_{\text{net}}| m_{\text{ion}}}{e_c} \tag{16}$$

where m_{ion} is the mass of the emitted ion species assuming it has a single charge. For positive charging, m_{ion} is replaced with m_{electron}, the mass of an electron, which is five orders of magnitude less than xenon gas ions. An advantage of using electrons is that they are essentially free propellant as they can be obtained on-orbit from solar energy. The instantaneous mass flow rate is directly proportional to the net plasma current and consequently power requirements and is computed for each plasma in a similar manner to Fig. 6. Table 2 lists the combined MC maximum mass flow rates for each of the plasma conditions. The maximum rates correspond to the extremes of the analyzed spacecraft potentials of ± 30 kV.

The maximum required mass flow rate occurs during the worst case, quiet plasma conditions ($\lambda_d = 4$ m) as the net plasma current to the craft is at its highest level then. In a nominal plasma ($\lambda_d = 200$ m) mass flow rates are reduced by at least an order of magnitude. The mass flow rates are orders of magnitudes lower for positive charging as low mass electrons are emitted. The currents here are still higher, so a higher electrical power is required compared to the negative charging.

The highest expected mass flow rate for this combined MC system are below 8 μg/s for all expected plasma conditions. The current spacecraft charge control technology can produce mass flow rates as high as 0.1 A at 100 μg/s and 10 A at 200 μg/s [25,28], indicating this is an achievable target with current technology. Also, the mass flow rate analysis conducted here does not account for any inefficiencies in the charge control device. In addition, the charge control accuracy for a TCS node system is not important, rather that the overall charge is significant to maintain tether tension and overcome external disturbances. For this reason, a higher mass flow rate increases the nodal charge and ultimately adds stiffness to the MC system.

C. Total Propellant Mass Comparison

For this MC TCS application example it is beneficial to estimate the total propellant mass required by the charge control system. The example used is the baseline MC system with spheres of 2 and 0.5 m radii. The nodes are operating in an orbit normal configuration at GEO with a desired center-to-center separation of 7 m. With a mother mass of 2000 kg and a child mass of 50 kg the differential gravity force compressing the craft has a magnitude of 74.4 μN. In this naturally compressive orbit scenario, the repulsive Coulomb force maintains a taut tether and desired situational awareness separation. To achieve this force in a nominal plasma requires the nodes to be charged to |12.2| kV. An advantage of the TCS concept here is that there is no need for sophisticated sensing and control. In addition there are no plume impingement concerns such as encountered if this scenario were implemented with free-flying craft with traditional chemical thrusters.

For the TCS system the total propellant mass is computed for both negative charging through emission of xenon ions (Xe^+) and positive charging with electron (e^-) emission using the mass flow rates of Table 2. The charge emission is used to apply continuous thrust to oppose the differential gravity force, maintaining the 7 m separation for 10 years. The propellant mass flow rate is computed for a nominal plasma ($\lambda_d = 200$ m) in sunlit conditions.

The total propellant mass requirements are extremely low for a Coulomb system. If operating in a nominal GEO plasma environment, the TCS system requires 122.4 g of xenon propellant for positive charging. For electrons the propellant requirement is only 0.0014 g. These propellant masses increase when considering inefficiencies of the system and variable plasma environments.

Another important consideration is the inert mass requirements of the charge control system. The charge control device inert mass is estimated to be low, in the low kg range, which matches well with current charge control technology as shown in the earlier charge control hardware section. As an example, charge control devices for current space missions have masses ranging from 19 kg on ATS-6 [29] through to the more recent Cluster devices weighing only 1.85 kg each [22,26]. These are devices that could be feasibly implemented on the mother and child craft.

VI. Child Mass Effects

As previously mentioned charge control can be conducted on both the mother and the child or only on one craft that transfers charge via the interconnecting tether. If charge control is conducted on the child craft, charging hardware and propellant requirements will impact the size and mass of the child spacecraft. However, with charge control mass requirements low the mass of the child craft will most likely be driven by what instruments it requires for operations. Analyzed here is the effect of various child masses on the relative dynamics of the baseline MC configuration. For launch purposes, minimal child mass is desirable, but at lower child masses the force induced from the charge control propellant emission may not be negligible. Because of this, a comparison of charge control emission force relative to the inflation Coulomb force is presented.

A. Relative Dynamics

Analyzed here is the effects of various masses on the relative dynamics of the MC TCS. Figure 10 shows the maximum relative rotations, maximum variation in separation distances and required control torques for various child masses. The results in Fig. 10 show that a lower mass child reduces the relative dynamics and required control torque of the mother. Figures 10a and 10b show that additional tethers provide increased stiffness of a MC TCS. However, similar to previous sections, multiple tethers have no effect on the required mother attitude control.

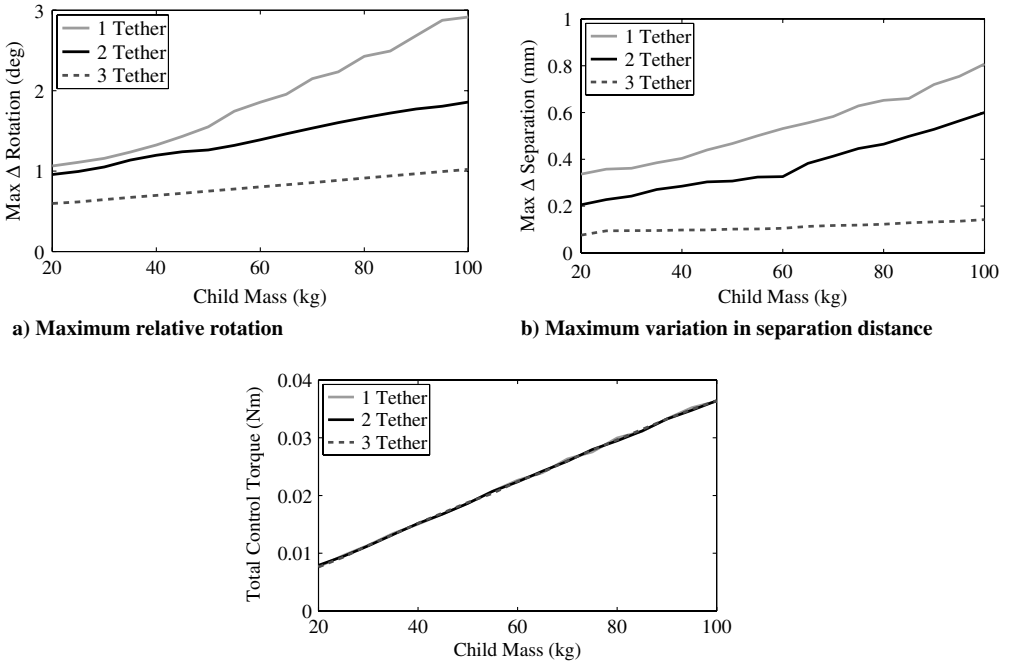

a) Maximum relative rotation

b) Maximum variation in separation distance

c) Total required attitude control torque

Fig. 10 MC relative dynamics as a function of child mass and number of connecting tethers.

B. Charge Emission Force and Node Accelerations

The charge current required to maintain a fixed potential is emitted under electrostatic acceleration. The emission current, while low magnitude, results in a net momentum exchange and consequently a force on the TCS nodes that feature charge control. In earlier studies this force is shown to be negligible for the free-flying charged spacecraft where Debye lengths are assumed to be at least 80 m or larger [3]. However, these Debye length values are not sufficiently conservative, hence the use of the worst case plasma conditions of this study ($\lambda_d = 4$ m). In addition, if a charge control device is implemented on the low mass child spacecraft it may experience relatively large accelerations due to the charge emission force. The charge-thrust force is computed for each of the plasma conditions and compared to the magnitude of the Coulomb force produced for the baseline MC system. The force on a node from the emission current is computed using [30]

$$F_{\text{cc}} = \dot{m} u_{\text{ion}} \tag{17}$$

where u_{ion} is the emission speed of the ions. During positive charging, low mass electrons are emitted. The mass flow rate is computed using Eq. (16) and the emitted ion species is assumed to be xenon here. The emission speed is proportional to the spacecraft potential V_{sc} and is calculated using electrostatic repulsion [30]:

$$u_{\text{ion}} = \sqrt{\frac{2 e_c V_{\text{sc}}}{m_{\text{ion}}}} \tag{18}$$

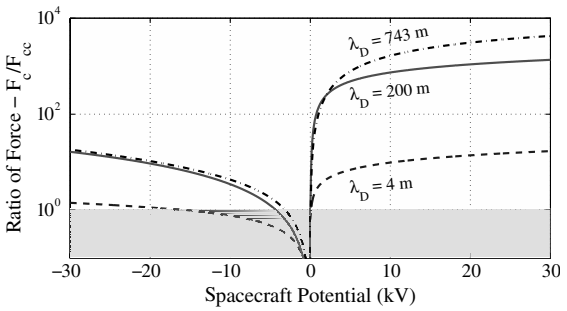

Fig. 11 Ratio of Coulomb force to charge emission force for the MC system in different plasmas.

Combining Eqs. (16–18) the net charge control force is computed with

$$F_{\text{cc}} = I_{\text{net}} \sqrt{\frac{2 m_{\text{ion}} V_{\text{sc}}}{e_c}} \tag{19}$$

The magnitude of the charge emission force is compared as a ratio of the Coulomb force and shown in Fig. 11. This total emission force is computed for both the mother and child combined in each of the three representative plasmas. The lower shaded region indicates where the charge emission force is greater than the Coulomb force at that potential.

It is desirable to have a large ratio between these forces given that the Coulomb force is our inflationary actuator and the charge emission force is seen as a potential disturbance on the system. For positive charging the emission of low mass electrons gives a suitably large ratio (>10 for the worst case plasma). However due to the higher momentum transfer of the xenon ions during negative charging the ratio between the forces is reduced. In the worst case plasma the forces are very similar magnitude. In the nominal and disturbed plasmas the charge emission force is approximately an order of magnitude less than the minimum Coulomb inflation force.

This study indicates that consideration for the placement and direction of the charge control device on the nodes should be made. If a single charge control device on the mother is used to charge the system, the emission force can be close or even greater than the Coulomb force magnitudes during negative charging and worst-case plasma conditions. With appropriate placement and the use of

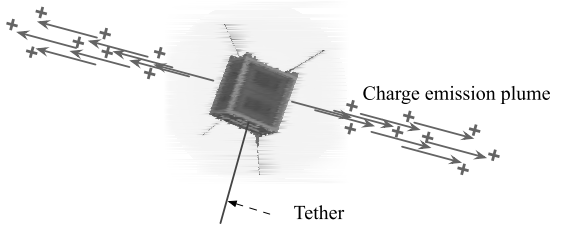

Fig. 12 Illustration of bidirectional charge emission on a tethered spacecraft node.

multiple emitters the emission force can be directed to create zero net force on the node and not interfere with Coulomb inflation forces. A conceptual example of a charged node with zero net force charge emission plumes is shown in Fig. 12. In addition, correct placement of the charge device on the mother or child could be used as an additional torque source to assist in controlling external perturbations such as gravity gradients.

VII. Conclusions

This paper analyzes the use of a tethered Coulomb structure (TCS) for situational awareness of a geosynchronous satellite by tethering a small child craft to a large mother craft. This study demonstrates that the mother–child (MC) TCS application provides a close proximity fixed sensor platform and is feasible for achievable charge and propellant mass requirements. By implementing a simple attitude control law on the mother craft, the formation can hold its orientation fixed relative to the orbit frame with minimal relative translation and rotation between the mother and the child. Using multiple tethers between the craft allows for separation distance of upwards of 10 m with relative rotations less than 5 deg.

Examination of the power required to maintain fixed potentials (up to ± 30 kV) shows that under nominal space weather conditions only watt levels of power are required. Variation of the spacecraft radius and polarity shows that larger radii craft and positive polarity charging requires more power. Additionally, simulations show that system stiffness increases rapidly with increasing potential until it plateaus around 30 kV.

Propellant mass requirements for the MC concept are directly related to the polarity of spacecraft charging. Negative charging requires several orders of magnitude larger propellant mass than positive charging because of the mass variation between electrons and ions. However, charging to negative potentials only requires 122.4 g of propellant for an example ten year mission, which is very comparable to other electric propulsion methods.

Lastly, this study examines various child masses and shows that lower mass improves the stiffness of the system by reducing relative translations, rotation, and required torque. However, lower child masses could result in nonnegligible accelerations being imposed on the child by the charging device. Even so, this acceleration could be harnessed and used to provide more system rigidity with intelligent spacecraft design.

References

[1] Tsuda, Y., Mori, O., Funase, R., Sawada, H., Yamamoto, T., Saiki, T., Endo, T., and Kawaguchi, J., "Flight Status of IKAROS Deep Space Solar Sail Demonstrator," *Acta Astronautica*, Vol. 69, Nos. 9–10, Nov.–Dec. 2011, pp. 833–840. doi:10.1016/j.actaastro.2011.06.005

[2] Schaub, H., and Junkins, J. L., *Analytical Mechanics of Space Systems*, 2nd ed., Education Series, AIAA, Reston, VA, 2009.

[3] King, L. B., Parker, G. G., Deshmukh, S., and Chong, J.-H., "Spacecraft Formation-Flying Using Inter-Vehicle Coulomb Forces," NASA Institute for Advanced Concepts (NIAC), Technical Rept., Jan. 2002.

[4] Schaub, H., Parker, G. G., and King, L. B., "Challenges and Prospects of Coulomb Spacecraft Formations," *Journal of the Astronautical Sciences*, Vol. 52, Nos. 1–2, Jan.–June 2004, pp. 169–193.

[5] Kong, E. M. C., Kwon, D. W., Schweighart, S. A., Elias, L. M., Sedwick, R. J., and Miller, D. W., "Electromagnetic Formation Flight for Multisatellite Arrays," *Journal of Spacecraft and Rockets*, Vol. 41, No. 4, July–Aug. 2004, pp. 659–666. doi:10.2514/1.2172

[6] Miller, D. W., Sedwick, R. J., Kong, E. M. C., and Schweighart, S., "Electromagnetic Formation Flight for Sparse Aperture Telescopes," *IEEE Aerospace Conference Proceedings*, Vol. 2, Big Sky, MT, 9–16 March 2002, pp. 2-729–2-741.

[7] Gersh, J., "Architecting the Very-Large-Aperture Flux-Pinned Space Telescope: A Scalable, Modular Optical Array with High Agility and Passively Stable Orbital Dynamics," AAS/AIAA Astrodynamics Specialist Conference, AIAA Paper 2008-7212, Honolulu, HI, 18–21 Aug. 2008.

[8] Peck, M. A., Streetman, B., Saaj, C. M., and Lappas, V., "Spacecraft Formation Flying Using Lorentz Forces," *Journal of the British Interplanetary Society*, Vol. 60, No. 7, July 2007, pp. 263–267.

[9] Schaub, H., Parker, G. G., and King, L. B., "Coulomb Thrusting Application Study," Virginia Tech and Aerophysics Inc., Dept. of Aerophysics, Technical Rept. No. A261344, Jan. 2006, p. 120.

[10] Seubert, C. R., and Schaub, H., "Tethered Coulomb Structures: Prospects and Challenges," *Journal of the Astronautical Sciences*, Vol. 57, Nos. 1–2, 2009, pp. 347–368.

[11] Seubert, C. R., and Schaub, H., "Rotational Stiffness Study of Two-Element Tethered Coulomb Structures," *Journal of Spacecraft and Rockets*, Vol. 48, No. 3, May–June 2011, pp. 488–497. doi:10.2514/1.49772

[12] Seubert, C. R., Panosian, S., and Schaub, H., "Attitude and Power Analysis of Multi-Tethered, Two-Node Tethered Coulomb Structures," *Journal of Spacecraft and Rockets*, Vol. 48, No. 6, Nov.–Dec. 2011, pp. 1033–1045. doi:10.2514/1.52185

[13] Bogorad, A., Bowman, C. K. Jr., Krummann, W. R., and Hart, W. R., "Spacecraft Solar Array Design to Control Differential Charging," U.S. Patent 5,919,316, 6 July 1999.

[14] Gurnett, D. A., and Bhattacharjee, A., *Introduction to Plasma Physics: With Space and Laboratory Applications*, Cambridge Univ. Press, New York, 2005, pp. 8–9.

[15] Whipple, E. C, "Potentials of Surfaces in Space," *Reports on Progress in Physics*, Vol. 44, No. 11, 1981, pp. 1197–1250. doi:10.1088/0034-4885/44/11/002

[16] Murdoch, N., Izzo, D., Bombardelli, C., Carnelli, I., Hilgers, A., and Rodgers, D., "Electrostatic Tractor 3 for Near Earth Object Deflection," *59th International Astronautical Congress*, IAC Paper 08-A3.I.5, Glasgow, 2008.

[17] Sliško, J., and Brito-Orta, R., "On Approximate Formulas for the Electrostatic Force Between Two Conducting Spheres," *American Journal of Physics*, Vol. 66, No. 4, April 1998, pp. 352–355. doi:10.1119/1.18864

[18] Smythe, W. R., *Static and Dynamic Electricity*, 3rd ed., McGraw–Hill, New York, 1968.

[19] Katz, I., Jongeward, G. A., Davis, V. A., Mandell, M. J., Kuharski, R. A., Lilley, J. R., Jr., Raitt, W. J., Cooke, D. L., Torbert, R. B., Larson, G., and Rau, D., "Structure of the Bipolar Plasma Sheath Generated by SPEAR I," *Journal of Geophysical Research*, Vol. 94, No. A2, Feb. 1989, pp. 1450–1458. doi:10.1029/JA094iA02p01450

[20] Olsen, R. C., Van Horn, T., Torbert, R., and Raitt, W. J., "SPEAR-1 Charging Behavior," *ESA Space Environment Analysis Workshop*, 9–12 Oct. 1990.

[21] Lai, S. T., and Tautz, M., "High-Level Spacecraft Charging at Geosynchronous Altitudes: A Statistical Study," *8th Spacecraft Charging Technology Conference*, Huntsville, AL, 20–24 Oct. 2003.

[22] Riedler, W., Torkar, K., Rudenauer, F., Fehringer, M., Pedersen, A., Schmidt, R., Grard, R. J. L., Arends, H., Narheim, B. T., Troim, J., Torbert, R., Olsen, R. C., Whipple, E., Goldstein, R., Valavanoglou, N., and Zhao, H., "Active Spacecraft Potential Control," *Space Science Reviews*, Vol. 79, Jan. 1997, pp. 271–302. doi:10.1023/A:1004921614592

[23] Deininger, W. D., Aston, G., and Pless, L. C., "Hollow-Cathode Plasma Source for Active Spacecraft Charge Control," *Review of Scientific Instruments*, Vol. 58, No. 6, June 1987, pp. 1053–1062. doi:10.1063/1.1139607

[24] Lai, S. T., "An Overview of Electron and Ion Beam Effects in Charging and Discharging of Spacecraft," *IEEE Transactions on Nuclear Science*, Vol. 36, No. 6, Dec. 1989, pp. 2027–2032. doi:10.1109/23.45401

[25] Aston, G. B., A. M., and Williams, J. D., "Miniature Plasma Activated Systems for Tether Current Generation," *Space Technology and Applications International Forum*, edited by American Institute of Physics, 2001.

[26] Torkar, K., Riedler, W., Escoubet, C. P., Fehringer, M., Schmidt, R., Grard, R. J. L., Arends, H., Rudenauer, F., Steiger, W., Narheim, B. T., Svenes, K., Torbert, R., Andre, M., Fazakerley, A., Goldstein, R., Olsen, R. C., Pedersen, A., Whipple, E., and Zhao, H., "Active Spacecraft Potential Control for Cluster: Implementation and First Results," *Annales Geophysicae*, Vol. 19, Nos. 10–12, 2001, pp. 1289–1302. doi:10.5194/angeo-19-1289-2001

[27] Torkar, K., Fehringer, M., Arends, H., Goldstein, R., Grard, R. J. L., Narheim, B. T., Olsen, R. C., Pedersen, A., Riedler, W., Rudenauer, F., Schmidt, R., Svenes, K., Whipple, E., Torbert, R., and Zhao, H., "Spacecraft Potential Control Using Indium Ion Source: Experience and Outlook Based on Six Years of Operation in Space," *Sixth*

Spacecraft Charging Control Technology Conference, AFRL-VS Paper TR-20001578, Hanscom AFB, MA, Sept. 2000.

[28] Marrese, C. M., "A Review of Field Emission Cathode Technologies for Electric Propulsion Systems and Instruments," *IEEE Aerospace Conference Proceedings*, Vol. 4, 2000, pp. 85–98.

[29] Shuman, B. M., Cohn, H. A., Hyman, J., Robson, R. R., Santoru, J., and Willamson, W. S., "Automatic Charge Control System for Geosynchronous Satellites," *Journal of Electrostatics*, Vol. 20, No. 1, 1987, pp. 141–154. doi:10.1016/0304-3886(87)90091-X

[30] Goebel, D. M., and Katz, I., *Fundamentals of Electric Propulsion*, JPL Space Science and Technology Series, Wiley, Hoboken, NJ, 2008.

A. Ketsdever
Associate Editor